J.G. Goldammer (Ed.)

Fire in the Tropical Biota

Ecosystem Processes and Global Challenges

With 116 Figures

Springer-Verlag Berlin Heidelberg New York
London Paris Tokyo Hong Kong Barcelona

Dr. Johann Georg Goldammer
Fire Ecology and Fire Management Research Unit
Institute of Forest Zoology
University of Freiburg
Bertoldstraße 17
7800 Freiburg, FRG

ISBN 3-540-52115-1 Springer-Verlag Berlin Heidelberg New York
ISBN 0-387-52115-1 Springer-Verlag New York Berlin Heidelberg

Library of Congress Cataloging-in-Publication Data. Fire in the tropical biota : ecosystem processes and global challenges / J.G. Goldammer (ed.). p.cm. -- (Ecological studies ; vol. 84) Papers from the Third Symposium on Fire Ecology held at Freiburg University in May 1989 and sponsored by the Volkswagen Foundation. Includes bibliographical references and index. ISBN 0-387-52115-1 (acidfree paper) 1. Fire ecology–Tropics–Congresses. 2. Wildfire–Tropics–Congresses. 3. Biotic communities–Tropics–Congresses. 4. Botany–Tropics–Congresses. 5. Fires–Tropics–Congresses. I. Goldammer, J.G. (Johann Georg), 1949- . II. Symposium on Fire Ecology (3rd : 1989: Freiburg University) III. Volkswagen Foundation. IV. Series: Ecological Studies ; v. 84. QH545.F5F575 1990 574.5'2623--dc20 90-10007

Printed in Germany

Typesetting: International Typesetters Inc., Makati, Philippines
2131/3145(3011)-543210 – Printed on acid-free paper

16 Remote Sensing of Biomass Burning in the Tropics

Y.J. KAUFMAN[1], A. SETZER[2], C. JUSTICE[3], C.J. TUCKER[4], M.C. PEREIRA[2] and I. FUNG[5]

16.1 Introduction

Biomass burning in the tropics, a large source of trace gases, has expanded drastically in the last decade due to increase in the controlled and uncontrolled deforestation in South America (Setzer et al. 1988; Malingreau and Tucker 1988), and due to an increase in the area of cultivated land with the expansion of population in Africa and South America (Seiler and Crutzen 1980; Houghton et al. 1987). In the burning process trace gases and particulates are emitted to the atmosphere, and the ability of the earth to fix CO_2 is substantially reduced (17% of the primary productivity occurs in the humid tropical forests – Atjay et al. 1979; Mooney et al. 1987), and as a result has a strong contribution to the anticipated climate change (Houghton and Woodwell 1989).

In the Amazon, as an example, a common practice associated with forest clearing and land management is the burning of the existing vegetation cover. Although these burnings occur in large numbers every year and have adverse effects on the environment, no estimates have been made to evaluate the magnitude of the problem. No official statistics exist for the extent of burning, and legal procedures to restrict or obtain authorization to burn the vegetation are seldom followed. Considering that the burning occurs in an area of many million square kilometers with poor road access, and that federal and state forest services are not suited to survey the forest, orbital sensing becomes the only practical technique to monitor the Amazon forest on a regular basis (Malingreau and Tucker 1988; Setzer and Pereira 1989; Kaufman et al. 1990).

An example of satellite-derived rate of deforestation is given in Fig. 1 for the state of Rondonia, Brazil (this figure is an expansion of the work of Malingreau and Tucker 1988). The deforestation in 1982 (see Fig. 1a) was much smaller than in 1987 (also in Fig. 1a). The rate of deforestation (per year) is shown in Fig. 1b. Although delayed in Rondonia, similar deforestation trends are found in other parts of the Amazon Basin (Setzer et al. 1988).

[1]NASA Goddard Space Flight Center, Greenbelt, Maryland 20771, also at University of Maryland, College Park, Maryland 20742, USA
[2]National Institute of Space Research (INPE), 12.201 Sao José dos Campos, Sao Paulo, Brazil
[3]NASA Goddard Space Flight Center, Greenbelt, Maryland 20771, also at University of Maryland, College Park, Maryland 20771, USA
[4]NASA Goddard Space Flight Center, Greenbelt, Maryland 20771, USA
[5]NASA Goddard Space Flight Center, Goddard Institute for Space Studies, New York, N.Y. 10025, USA

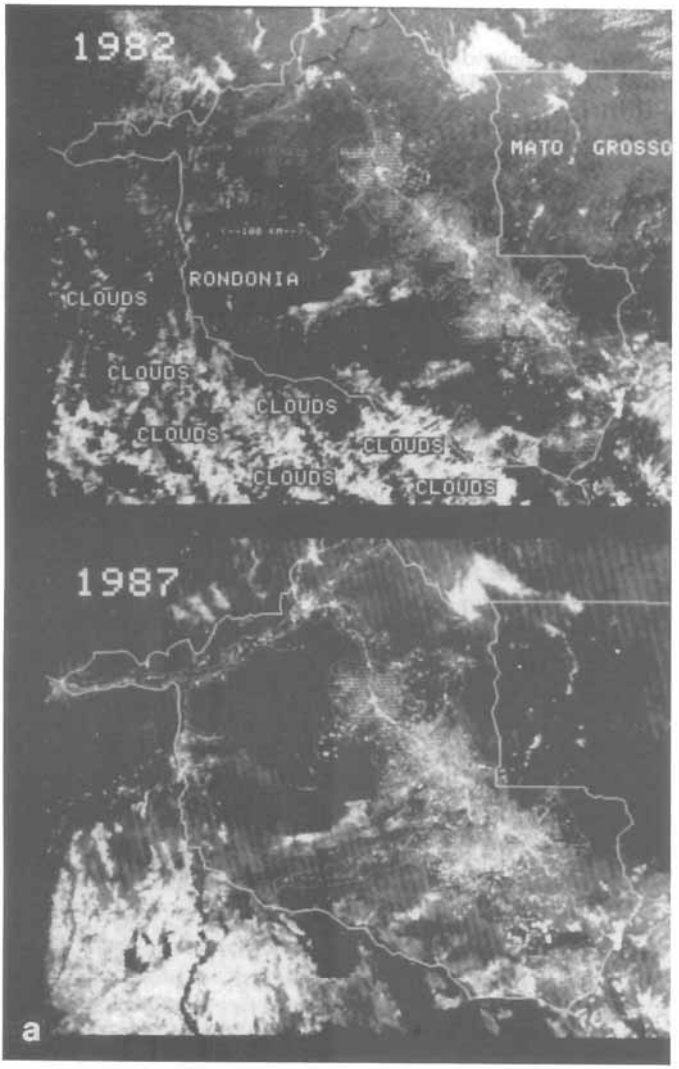

Fig. 1. Rate of deforestation (per year) in the state of Rondonia, Brazil. **a** Deforestation in 1982 and 1987, shown by the response in AVHRR channel 3 (3.7 μm). **b** Accumulated deforestation

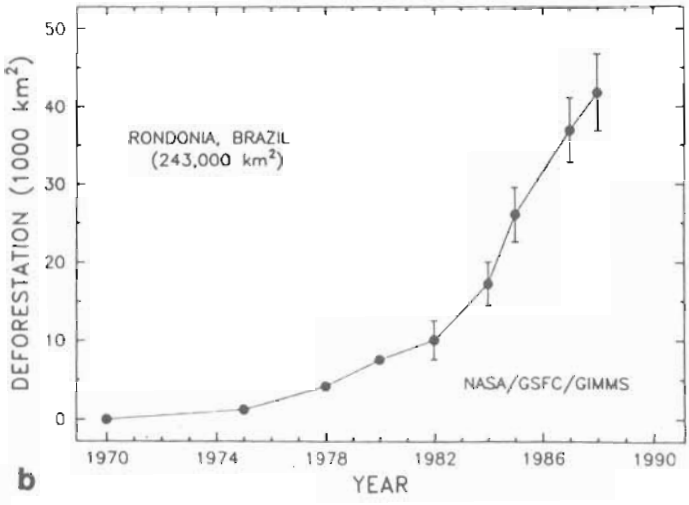

Fig. 1b.

The rationale for the study of biomass burning is linked to the need of the Global Tropospheric Chemistry program (GTC 1986) to understand the sources and sinks of the atmospheric trace gases and their variations in the atmosphere. The importance of the trace gases other than CO_2 (e.g., CH_4 and CO) is in their greenhouse effect, which is comparable to that of CO_2 (Ramanathan et al. 1985), and in their effect on tropospheric chemistry (Crutzen 1988). We shall concentrate in this chapter mainly on remote sensing of trace gases other than CO_2, since biomass burning is generally an inefficient combustion and the relative abundance of trace gases is high. Trace gases also play an important role in atmospheric chemistry, whereas CO_2 is completely oxidized.

Removal of the trace gases from the atmosphere is mainly by oxidation processes. Measurements of the emission rates of trace gases can show the potential of changes in the atmospheric balance. Comparison of the changes of the emission rates with the variations in the background concentration can teach us about the ability of the atmosphere to take care of extra emission, i.e., the cleansing process. For example, methane (CH_4) concentration is increasing by 1% a year (GTC 1986; Blake and Rowland 1986) and has doubled in concentration over the last 100–300 years after being constant for thousands of years (Stauffer et al. 1985). It is not clear whether this increase is due to an increase in the emission of CH_4, a reduction in the oxidation of methane (GTC 1986), and/or an increase in the conversion of other organic gases to methane. The present increase in the tropospheric concentration of ozone (an oxidant), not only in strongly polluted areas (Fishman and Larsen 1987), but also at background stations (Oltmans and Komhyr 1986), suggest that there cannot be a reduction in the oxidation process, and the increase in the methane concentration has to be explained by an increase in the methane emission. The larger seasonal cycles in the CH_4 concentrations in the Northern Hemisphere than in

the Southern Hemisphere also suggest the dependence of CH_4 concentration on source variation.

During prescribed and natural fires large amounts of trace gases (e.g., CO_2, CO, CH_4, NO_x) and particles (organic matter, graphitic carbon, and other constituents) are released to the atmosphere. It is estimated that biomass burning contributes 5–30% of the global amounts of CH_3Cl, CH_4, NO_2 (GTC 1986; Crutzen and Graedel 1988) thus having a similar contribution to the atmospheric trace gases as fossil fuel burning (Crutzen et al. 1985; Fishman et al. 1986) and more than half of the contribution of fossil fuel in CO_2 (Seiler and Crutzen 1980; Crutzen et al. 1985; Mooney et al. 1987). It increases the atmospheric greenhouse effect as well as affecting tropospheric chemistry (Crutzen et al. 1979). Trace gases such as N_2O and CH_4, which are stable in the troposphere, can penetrate to the stratosphere, be activated by UV radiation, and affect the chemistry of the stratosphere (Crutzen et al. 1985). There is also evidence of an increased production of N_2O from soil following fires (Anderson et al. 1988). Note that most of the stratospheric NO, that serves as a catalyst in the ozone destruction, originates from tropospheric N_2O (Wayne 1985). NO is responsible for about 70% of the annual global destruction of stratospheric ozone via the nitrogen oxide catalytic cycle (Turco 1985; Cofer et al. 1988). One radiatively active trace species, ozone, is not emitted directly by burning, but despite its secondary nature, it may be affected as strongly by tropical burning as methane or aerosol. Observations made in situ (Crutzen et al. 1985; Andreae et al. 1988) and from space (Fishman and Larsen 1987) suggest that high ozone in the continental tropics, forested or agricultural ecosystems, is most likely associated with burning emissions of pollutants. The fires emit NO, and extrapolation of studies of mid-latitude, predominantly urban pollution (Seinfeld 1986) suggests that it is the NO emission that is most important in the tropics for ozone production (Chatfield and Delany 1988).

The particles emitted from biomass burning may affect the radiation budget and boundary layer meteorology by reflecting sunlight to space and absorbing solar radiation (Coakley et al. 1983). The particles emitted from biomass burning are a major source of cloud condensation nuclei (Radke 1989). Therefore an increase in the aerosol concentration may cause an increase in the reflectance of thin to moderate clouds (Twomey 1977; Coakley et al. 1987) and a decrease in the reflectance of thick clouds (Twomey et al. 1984). Since for most clouds the aerosol effect dominates through an increase in the cloud albedo, Twomey et al. (1984) suggested that the net cooling effect due to the increase in the aerosol concentration can be as strong as the heating effect due to the increase of global CO_2 and other trace gases, but act in the opposite direction (Coakley et al. 1987). Therefore, the net effect of increased concentration of aerosol and trace gases on the earth's energy budget is not obvious.

Biomass burning in the tropics is of particular interest, due to the large extent of forest clearing and agricultural burning. Estimates based on satellite imagery are of 350,000 fires corresponding possibly to 200,000 km^2 of burned vegetation in Brazil's Amazon alone (Setzer et al. 1988; Setzer and Pereira 1989). Biomass burning is also important due to the high solar irradiation in the tropics,

that enhances atmospheric chemical reactions (due to the U.V. radiation) and the aerosol climatic effects (more solar radiation to be reflected to space). In addition to the study of the emission of trace gases, it is also important to monitor the emission of the particles, due to their possibly strong, but poorly understood effect on climate (through cloud modification), and their ability to serve as the surface for heterogeneous atmospheric chemistry.

Present methods for the estimation of trace gas emissions from biomass burning are based on measurements of the ratio of the trace gas concentration to the concentration of CO_2 (Andreae et al. 1988), and on a crude global estimate of the rate of emission of CO_2 during biomass burning (Seiler and Crutzen 1980). This estimate may suffer from uncertainty in the overall extent of biomass burning, e.g., rate of deforestation, or agricultural burning practices, and in the density of the burned material. As a result, it is very important to obtain direct information about the fires and the emission products. Satellite imagery provides such an observational tool. It can show the spatial and temporal distribution of fires (at least the ones that are observable during the satellite pass) and provide a measure of the rate of deforestation (Tucker et al. 1984; Malingreau and Tucker 1988), as well as measure one emission product – the emission of particles from the fires (Kaufman et al. 1989). Although satellite imagery cannot be used directly to sense the emitted trace gases, both the mass of emitted particles and the mass of emitted trace gases are proportional to the mass of the burned biomass. In Figs. 2 and 3, the relation between the emitted trace gases and particulates is shown, based on the measurements of Ward (1986) of the mass of the emitted species per unit area of the fire. Due to the variability of the density of the consumed fuel in each case, a strong relation is observed between the trace gases and CO_2 (Fig. 2) or particulates (Fig. 3). Ward (1986) also normalized the emission measurements for the mass of fuel (see Figs. 4 and 5). The normalized emission ratios show the relations between the different emission species, due to variability of the fire efficiency. The correlation between methane emission (CH_4) and particulate emission (see Figs. 3 and 5) shows that estimate of methane emission can be more accurately done from particulate measurements than from fuel consumption measurements.

Once the relationship among the emitted particles, trace gases, and the burned biomass is established (for a given land cover) measurement of the emitted particles can be used to determine the mass of the emitted trace gases, and to some extent, the mass of the emitted CO_2. For example, CH_4 and CO can be computed directly from the measured mass of particles using the relationship between them (Figs. 3 or 5), while N_2O can be computed from the mass of emitted CO_2, using a conversion ratio measured by Cofer et al. (1988) of 0.0002 between the mass of emitted N_2O and the mass of emitted CO_2.

Among satellites that can be used to monitor large fires, the meteorological NOAA series of polar orbiters present a unique capability: daily coverage currently by two satellites with at least four daytime and four nighttime passes for any area; multispectral coverage with the same 1.1 km resolution in visible, near, and thermal infrared bands; and a relatively easy capability of near-real time receiving and processing of images covering areas of continental dimen-

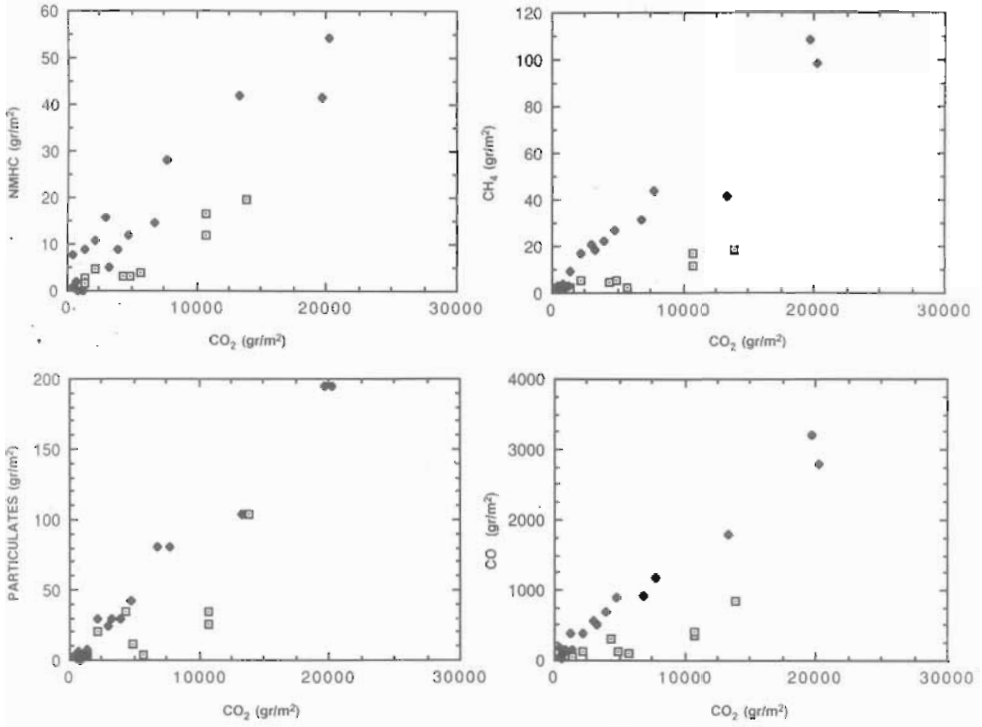

Fig. 2. The relation between emission of CH_4, NMHC, particles and CO and the emission of CO_2 in g of the emitted substance to m^2 of the burned area. Data are taken from Ward (1986) for flaming (□) and smoldering (♦) conditions

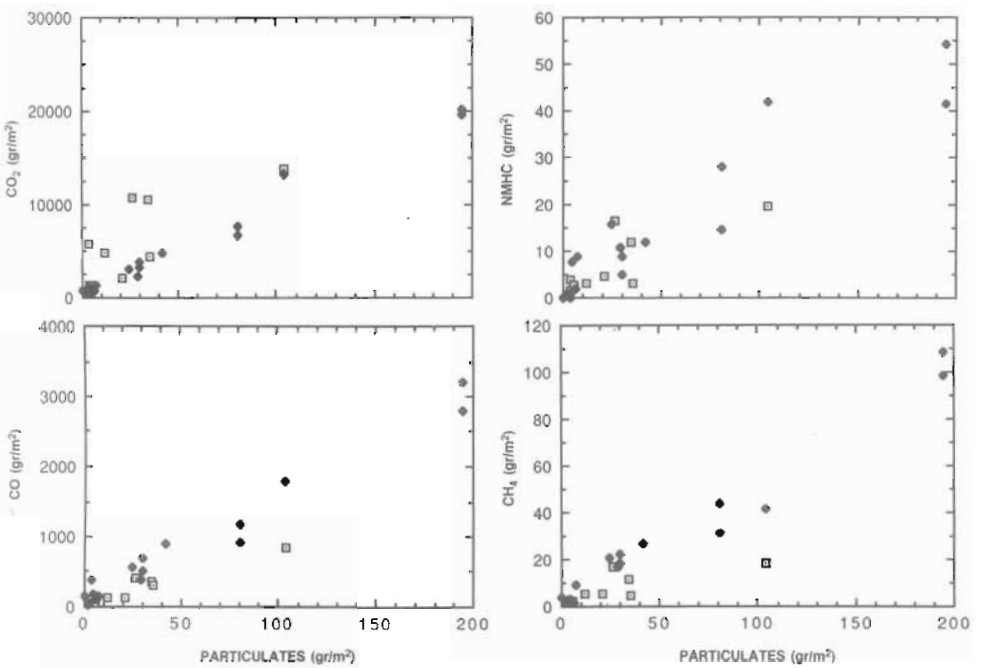

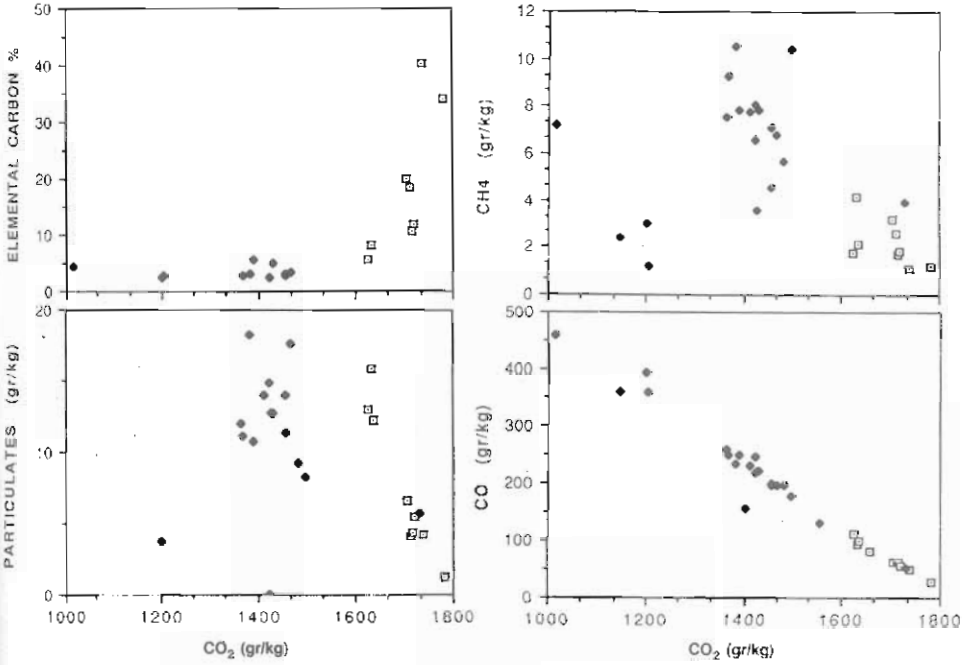

Fig. 4. The relation between emission of elemental carbon, CH_4, particles and CO and the emission of CO_2 in units of the ratio of mass of the emitted substance to the mass of burned fuel. Data are taken from Ward (1986) for flaming (□) and smoldering (♦) conditions

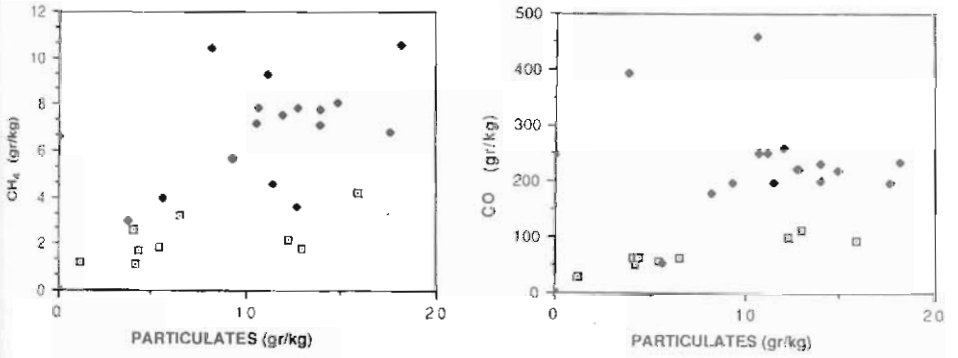

Fig. 5. The relation between emission of CO and particles, and CH_4 and particles (in units of the ratio of mass of the emitted substance to the mass of burned fuel). Data are taken from Ward (1986) for flaming (□) and smoldering (♦) conditions

Fig. 3. The relation between emission of CO, CO_2, CH_4, and NMHC and the emission of particles (in gram of the emitted substance to m^2 of the burned area). Data are taken from Ward (1986) for flaming (□) and smoldering (♦) conditions

sions. LANDSAT TM and SPOT (30 and 10 m resolution, respectively) can also be used and provide much finer details of the fires and burning areas, but such systems are of limited use for regional monitoring due to the high data volumes associated with the high spatial resolution and low temporal repeat frequency of many days.

16.2 The NOAA-AVHRR Series

The NOAA-AVHRR series provides a set of images in five spectral bands (four AVHRR passes are available daily). Its visible (0.63 μm) and near-IR (0.85 μm) channels can provide information (during the day) on the surface characteristics and the smoke loading and characteristics (Kaufman et al. 1990; Ferrare et al. 1990). The 3.7-and 11-μm channels can be used, during day and night, to monitor the number and spatial distribution of the fires. Therefore it should be an adequate tool for regional and global remote sensing of fires and their emissions. The analysis of AVHRR bands 1 and 2 requires accurate satellite calibration (less than 10% absolute error, less than 1% change during a 20-day period and less than 5% error in relative calibration between the channels (Kaufman et al. 1990). Presently, the AVHRR first two channels are calibrated using radiances measured over remote ocean areas and deserts (Kaufman and Holben 1990) and by an aircraft-calibrated scanning radiometer above White Sands National Monument in New Mexico (B. Guenther pers. commun.). It is expected that with these calibrations such requirements can be met.

A preliminary operational scheme for monitoring biomass burning using 1-km data from the AVHRR system was devised by the Brazilian Space Institute (INPE/MCT) for the 1987 Amazon burning season. The afternoon pass of the NOAA-9 was recorded by INPE over central South America. The images were processed on the day of recording to detect large forest burnings, and by the following day the geographical location of the main fires was available to state representatives of the Brazilian Institute of Forest Development (IBDF/MA).

16.3 Remote Sensing of Fires, Smoke, and Trace Gases

The radiative temperature of the pixel from AVHRR channels at 3.7 and 11 μm can be used to identify fires (Dozier 1980; Matson and Dozier 1981; Matson et al. 1987). Since the fire line cannot fill a pixel, we may consider the pixels to be only partially filled with fires. Although for some hot objects the two channels can be used to identify the hot object temperature and its subpixel size, for fires (temperature > 500 K), even if 0.01–0.1% of the pixel is covered by a fire it is enough to saturate the 3.7 μm channel of the AVHRR, and have a small effect in the 11 μm channel (see Fig. 6). The AVHRR sensor was not designed for fire monitoring and both AVHRR channels saturate around 320 K (Matson et al.

carbon is released than under smoldering conditions. Graphitic carbon is a very strong absorber of light in the solar spectrum, and therefore ω_0 is around 0.97 for smoldering and as low as 0.66 for flaming conditions (Patterson and McMahon 1984). Measurements of the aerosol absorption in field fires (Patterson et al. 1986) showed a much smaller range of variation that corresponds to ω_0 in the range 0.90–0.96. Radke et al. (1988) used aircraft sampling to find a variation in ω_0 from 0.75 for a strong fire of dry wood to 0.82–0.91 for typical large prescribed fires (Radke et al. 1988). Measurements of total emitted particulates mass and graphitic carbon (Andreae et al. 1988) in the Amazon basin show that 7% of the particulates is graphitic carbon which corresponds to $\omega_0 \sim 0.96$ and indicates a large portion of smoldering in the emission.

Given current sensor capability, satellites cannot observe directly the emitted trace gases in the lower troposphere. Only concentration of tropospheric ozone (Fishman et al. 1986; Fishman and Larsen 1987) was derived indirectly by subtracting from the total ozone estimated from the TOMS (Total Ozone Mapping Spectrometer) data and stratospheric ozone derived from the SAGE (Stratospheric Aerosol and Gas Experiment) experiment. Therefore, in order to obtain information about the emission products from fires, a remote sensing method is proposed that concentrates on detection of fires and remote sensing of the emitted particles, and translation of these observations into trace gas emission using measured ratio of particle concentrations and trace gas concentrations in the smoke for several fire conditions (see Figs. 3 and 5). Alternatively, the number of fires can be used to estimate the trace gases emission by using measurements of the burned biomass in an "average" fire and average ratios between the emitted trace gases and the emitted CO_2.

The data of Ward and Hardy (1984) and Ward (1986) indicates that there is a strong relationship between particulate matter emission (M_{part}) and CH_4 emission (M_{CH_4}), see Fig. 3. The relation is somewhat different for flaming or smoldering:

$$M_{CH_4} = 0.6 M_{part} \quad \text{for smoldering conditions, and} \quad (1)$$

$$M_{CH_4} = 0.3\, M_{part} \quad \text{for flaming conditions.} \quad (2)$$

M_{CH_4} can be derived from M_{part} with uncertainty of 20% if the stage of the fire is determined, and 50% if it is not (see Fig. 3). Similar relations were found for NMHC:

$$M_{NMHC} = 0.3 M_{part} \quad \text{for smoldering conditions, and} \quad (3)$$

$$M_{NMHC} = 0.2 M_{part} \quad \text{for flaming conditions.} \quad (4)$$

For CO similar relations were found, except that the emission of CO is better correlated with the emission of CO_2 (see Fig. 4), than with the emission of particles for the smoldering phase. Nevertheless, CO can also be determined from the derived particulate mass with similar uncertainties (see Figs. 3 and 5). The measurements of Ward (1986, see Fig. 5) indicate that the relations between CO and particles emission are:

$$M_{CO} = (17 \pm 5)M_{part} \quad \text{for smoldering conditions, and} \quad (5)$$
$$M_{CO} = (10 \pm 5)M_{part} \quad \text{for flaming conditions.} \quad (6)$$

Since particulate matter concentrations in the atmosphere can be derived from satellite imagery (Fraser et al. 1984; Kaufman and Sendra 1988a,b; Kaufman 1987), therefore the mass of CH_4, CO and other trace gases can be derived as well. The relationship between the emission of particulates and the emission of CO_2 can also be found from Fig. 4 (data of Ward 1986) as:

$$M_{CO2} = (100 \pm 30)M_{part} \quad \text{for smoldering conditions, and} \quad (7)$$
$$M_{CO2} = (170 \pm 80)M_{part} \quad \text{for flaming conditions.} \quad (8)$$

It is not completely clear at this point how well these relationships represent the conditions found in the tropics. Measurements of emitted trace gases were performed in Brazil (Greenberg et al. 1984; Crutzen et al. 1985; Andreae et al. 1988) but the concentration of submicron aerosols was not measured. Greenberg et al. (1984) measured the relation between the emitted CH_4 and CO and the emitted CO_2. They found that the volume ratio of CO and CO_2: V_{CO}/V_{CO2} is 0.12 (range between 0.05 and 0.30) which corresponds to mass ratio M_{CO}/M_{CO2} of 0.08 (range between 0.03 and 0.20). It is assumed here that the low part of that range corresponds to flaming conditions, while the upper part of the range to smoldering conditions, similar to the measurements of Ward (1986) shown in Fig. 4). This range of mass ratio results in production rate for CO of 50 (g kg^{-1} fuel) for flaming and 280 (g kg^{-1} fuel) for smoldering. These production rates are similar (within 30%) to the production rates measured by Ward (1986) and presented in Fig. 4. Table 1 summarizes these results. For comparison, the derived rates from the volume ratios measured by Andreae et al. (1988) for mixed smoldering/flaming conditions result in emission rates smaller than the above (see Table 1). A similar comparison is carried for CH_4 in Table 1, resulting in a similar fit. The variation between the measurements of Greenberg et al. (1984), Ward (1986), and Andreae et al. (1988) results from different fuel and fire characteristics. By using the ratio between CH_4 and aerosol and between CO and aerosol, this variation can be decreased, since all these three biomass burning products are released in larger quantities with the reduction of the fire efficiency (which is not true for CO_2).

Water vapor condensation on the aerosol particles may result in an uncertain estimate of the nonwater part of the emitted particles. The moisture contained in the biomass and water generated through combustion can make only a small increase in the relative humidity of the smoke (Ward et al. 1979). Most of the water vapor in the smoke was in the ambient air before the fire. Therefore, the effect of water vapor on aerosol scattering characteristics depends on the atmospheric profile of the relative humidity and the altitude of the smoke. Andreae et al. (1988) found that in the Amazon Basin the smoke was emitted in thin layers located 1–4 km from the ground. In the relatively dry conditions in the fire season, the relative humidity in the lowest 4 km is between 40 and 70% for savannah and 50 and 85% for tropical forest regions (Crutzen et al. 1985). Hänel

Table 1. Comparison between production rates for CO and CH_4

Quantity and source	Smoldering	Flaming	Mixed
M_{CO}/M_{CO_2}[1]	0.20	0.03	0.08
CO_2 production rate (g kg^{-1} fuel)[2]	1400	1700	1550
CO resultant production rate (g kg^{-1} fuel)	280	50	120
M_{CO}/M_{CO_2}[3]			0.056
CO resultant production rate (g kg^{-1} fuel)			85
M_{CO}/M_{CO_2}[4]			0.09
CO resultant production rate (g kg^{-1} fuel)			140
CO production rate (g kg^{-1} fuel)[2]	220	70	150
M_{CH_4}/M_{CO_2}[1]	0.008	0.002	0.004
CO_2 production rate (g kg^{-1} fuel)[2]	1400	1700	1550
CH_4 resultant production rate (g kg^{-1} fuel)	11	3.5	6
CH_4 production rate (g kg^{-1} fuel)[2]	7	2	5

[1] Greenberg et al. (1984), [3] Ward (1986) and Fig. 4, [3] Andreae et al. (1988), [4] Crutzen et al. (1985).

(1981) developed a model of the relationship between relative humidity and particle size. According to this model, for a relative humidity of 70%, it is expected that roughly 50% of the particulate mass will be water, as long as there is no saturation (see also Kaufman et al. 1986). Saturation can be detected as cloud formation resulting in high spatial nonuniformity in the smoke. We estimate that the error in the derivation of the dry aerosol mass due to the error in the humidity effect is $\pm$ 30%.

16.4 Remote Sensing of Aerosol Characteristics

Satellite imagery of the earth's surface in the visible and near-IR part of the spectrum were used to derive the aerosol optical thickness (a measure of the aerosol mass loading in the atmosphere), its single scattering albedo (ratio between scattering and total extinction – a measure of the presence of graphitic carbon in the aerosol) and the particle mass median size. The remote sensing technique is based on the difference in the upward radiance, reaching the satellite sensor, between a hazy day and a clear day (Fraser et al. 1984; Kaufman 1987; Kaufman et al. 1990; Ferrare et al. 1990). The aerosol optical thickness can be detected from the radiances above water or land for most land covers (except bright soil or sand). The single scattering albedo can be detected over a sharp contrast in the surface reflectance, e.g., a sea shore as well as over vegetated areas (here the contrast is between the low reflectance in the visible and the high reflectance in the near IR). The particle size is derived from the wavelength dependence of the optical thickness. The aerosol optical thickness can be detected in AVHRR imagery in more than one wavelength only over water. Therefore, the particle size can be derived only from images acquired over water. Derivation of the aerosol optical thickness using a single image was

applied by Kaufman and Sendra (1988a,b) over forests. The methods were applied to GOES (Fraser et al. 1984), AVHRR (Kaufman et al. 1990; Ferrare et al. 1989) and LANDSAT MSS imagery (Kaufman and Sendra 1988a,b). The derived aerosol optical thickness was verified by sunphotometer measurements from the ground (Fraser et al. 1984; Kaufman and Sendra 1988a,b). The derivation of the single scattering albedo was tested in a laboratory simulation (Mekler et al. 1984; Kaufman 1987).

16.5 Satellite Estimation of Gaseous Emission from Biomass Burning

The remote sensing techniques are based on the analysis of NOAA-AVHRR 1 km resolution imagery. The 3.7-μm and the 11-μm channels are used to detect fires and distinguish them from clouds and hot soil (that may also saturate the 3.7-μm channel). The mass of particulates in the smoke and their single scattering albedo (ω_o) are determined from the visible and near-IR channels (ω_o is used to distinguish between the relative contribution of smoldering and flaming to the smoke). In the following sections two methods for the remote sensing of the emitted trace gases are applied. In the next section, the average emission of particulates per fire is determined from the satellite imagery, and converted to the emission of trace gases by Eqs (1)–(8). The total emission is found by multiplying by the total number of fires. In Section 16.5.2, the total number of fires is used to compute the total burned biomass using the amount of biomass burned in an "average fire". The amount of burned biomass is converted into the emitted trace gases using emission rates from the literature.

16.5.1 Estimate Based on the Average Emission of Particulates per Fire

Since fires are better spatially defined in the image than smoke, first the average emission of particulates per fire (in a given area and season) is estimated and the corresponding total amount of fires (in the same season and area) is computed. The total mass of the emitted particulates is computed as a product of the emitted mass per fire and the total number of fires. This indirect procedure has two advantages. Statistically, it surveys the area by counting fires, that due to their distinct spatial nature are more easily defined than smoke. On the other hand, the disadvantages in counting fires (we cannot distinguish between large and small fires, we may miss very small fires or fires that were extinguished before the satellite pass) are eliminated by the fact that in the procedure we first divide by the number of fires in a given area and day to find the emission per fire, and then multiply by the total number of fires to find the total emission. In this way the subjectivity of defining fires by the satellite capability is canceled in the process. The mass of the emitted particulates is converted to the mass of emitted trace gases and CO_2.

16.5.1.1 Basic Assumptions

The basic assumptions in the remote sensing analysis are the following:

- For each land management zone and season it is possible to define an "average fire" so that if the characteristics of a large sample of fires are established, the total emitted mass of particles and trace gases can be found from the total number of fires.
- The relations between the emission rate of particles, trace gases, CO_2, and the mass of burned biomass, that are found from prescribed fires (Ward and Hardy 1984; Ward 1986) can be applied to the fires in the tropics and other regions of the world. In this regard it is helpful that the fires monitored by Ward and others consumed different types of wood and were carried in varying meteorological conditions (Ward 1986).
- There is a direct relationship between the particulate characteristics measured by Ward (1986) and the particulate characteristics measured from space. The relation between the mass of particles measured from the ground and derived from satellite radiances were discussed by Fraser et al. (1984). Past measurements of particles and gases made using sampling devices suspended from towers have compared favorably with measurements made using airborne sampling techniques (Ward et al. 1979).
- It is possible to separate the contribution of liquid water and the emitted material from the fire to the light scattered by the smoke. The contribution of the liquid water is found from climatology of the area as well as from local meteorological information.
- It is possible to assume a value of the refractive index and size distribution of the particles.

16.5.1.2 Estimation of the Emission Rates per Fire

For a given land cover category and season, it is assumed that the range of fires and resulting emissions can be represented by an average fire. To find the emissions from an average fire, the emitted smoke has to be related to the fires from which it is emitted. For this purpose, an area in the satellite image is determined for which there is a direct relation between the smoke and the fires that emitted the smoke (see Fig. 7). The average rate of emission and characteristics of the aerosol part of the smoke is estimated from AVHRR channels 1 and 2. These two reflective channels are calibrated using the calibration of Kaufman and Holben (1990). The aerosol optical thickness is computed from the difference in the radiances in channel 1 between the area that contains the smoke and a nearby background radiance. The integrated mass of smoke is computed from the derived optical thickness, integrated on the area covered by the smoke. A conversion factor is used to convert the optical thickness into the mass of aerosol per unit area of the surface. For the assumed average particle radius (averaged on the mass distribution) of 0.3 μm, the conversion factor is 0.22

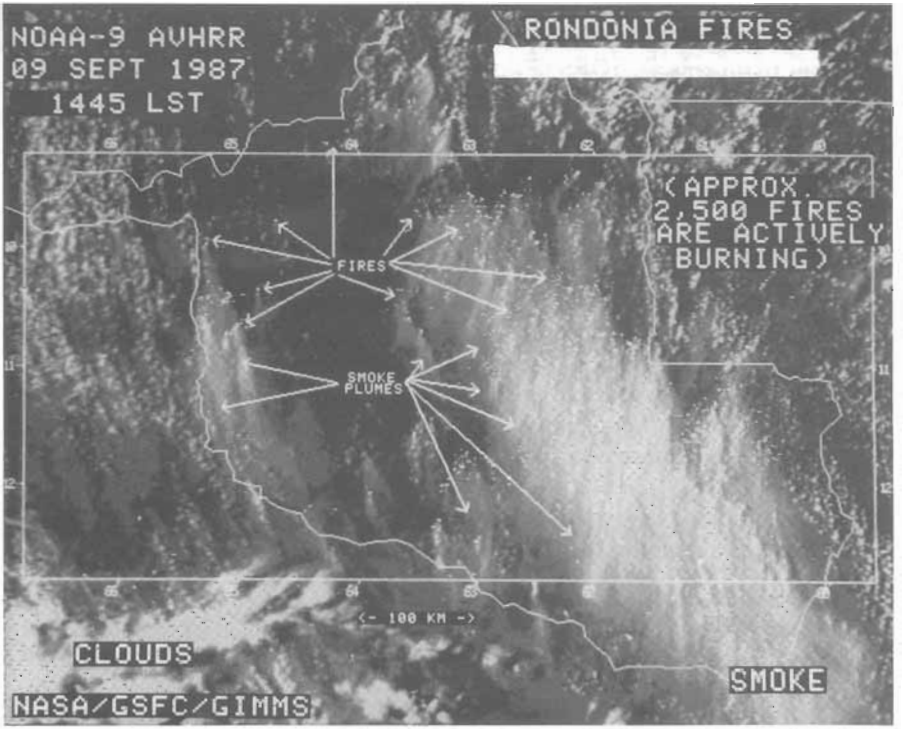

Fig. 7. The fires and smoke of biomass burning due to deforestation in the state of Rondonia, Brazil. The image was generated from AVHRR channels 1–4. Fires are shown by *white dots* (based mainly on the radiance in channel 3–3.7 μm), vegetation is *dark* (based on the radiance in channels 1–0.63 μm and 2–0.85 μm), smoke is *gray* (channels 1 and 2) and thick clouds are *white* (channels 1, 2, and 4–11 μm). The latitude and longitude lines are indicated. In the image there are 1500 fires and as a result, heavy smoke covers 50,000 km²

g m^{-2} (assuming density of 1 g cm^{-3}). This particle radius of the emitted smoke is taken as the average of the radius measured in situ (Radke et al. 1988) and by remote sensing (Puschel et al. 1988; Kaufman et al. 1990; Ferrare et al. 1990). For comparison Tangren, (1982) derived a value of 0.28 g m^{-2} from a comparison of particulate mass and a nephelometer scattering coefficient. Since our remote sensing method is sensitive only to small particulates (less than 2 μm) it is reasonable to use a somewhat smaller value. If half of the aerosol mass is liquid water (see discussion in Sect. 16.3), then the conversion factor from the aerosol optical thickness to the dry aerosol mass is 0.11 g m^{-2}.

The value of ω_o (the single scattering albedo) is determined from the relation between the increase in the upward radiance, due to the presence of the smoke, in channel 1 and channel 2 (Fraser and Kaufman 1985; Kaufman 1987; Kaufman et al. 1990; Ferrare et al. 1989) and is used to estimate the relative contribution of smoldering and flaming phases to the total emissions. Since the AVHRR can measure the smoke release only once or twice a day (morning and

afternoon passes), there is a need to estimate the relation between the smoke seen from the AVHRR and the actual daily generation of smoke, from more frequent platforms – GOES (Fraser et al. 1984) and/or ground observations (Kaufman and Fraser 1983). Cloud analysis from the AVHRR is used to estimate the effect of clouds on fire detection and the effect of condensation and cloud generation on the aerosol. The following is the algorithm to estimate the emission of particulates per fire:

1. From GOES and/or ground observations estimate the ratio t_{fire}/t_{avhrr} where t_{fire} is the average daily duration of most of the emission and t_{avhrr} is the duration of substantial emission till the AVHRR image is taken.
2. From the AVHRR find the total dry mass of the smoke M_a in a given area, the average value of ω_o and the number of fires that contribute to this smoke.
3. Estimate the fractional contribution of flaming and smoldering to the smoke from ω_o, then estimate the emission ratios $C_{CH4}(\omega_o)$, $C_{CO}(\omega_o)$, etc.
4. Compute the emitted mass M_{CH4}, M_{CO}, M_{af} (total dry aerosol mass) etc: $M_i = (t_{fire}/t_{avhrr})*M_a* C_i(\omega_o)$, where i is CH_4, CO etc.
5. Compute the average emission of particles and gases per fire (by dividing the emitted mass by the number of fires).

In 1987 the AVHRR afternoon pass was around 15.30 h LST. Assuming that the fires start around 11.00–12.00 h LST and produce most of the emission in 7 h, then the ratio is t_{fire}/t_{avhrr} and 0.5 ± 0.2.

16.5.1.3 Remote Sensing of Fires and Total Emitted Mass

The radiative temperature of the pixel from AVHRR channels at 3.7 and 11 μm is used to identify fires. The 11 μm channel is used to distinguish between fires, reflective clouds, and hot surface areas. A hot surface ($320 < T < 400$ K) will saturate both the 11 μm and the 3.7 μm channels. For pixels that include fires, the radiance in the 3.7 μm channel will be much larger than in the 11 μm channel and usually saturated (see Fig. 6). Water clouds that saturate the 3.7 μm channel, will usually result in low radiances in the 11 μm channel, and have an irregular shape. A computer program determines the amount of fires, based on these criteria (see Sect. 16.5.1.4 for details).

The total emission during the fire season is computed by multiplying the emission per fire by the number of fires. The emission is adjusted for the cloudiness (that covers some of the fires) by the cloud fraction. The cloud fraction is found from the satellite images, based on a threshold reflectance in the visible band.

16.5.1.4 Accuracy Estimates

The process of computation of the particles and trace gases emission involves several steps (as discussed in the previous paragraphs). In the following the errors in each step are estimated:

- Computation of optical thickness from the detected radiances – 30% error (Fraser et al. 1984).
- Computation of the total aerosol mass from the optical thickness – 30% error (Fraser et al. 1984).
- Computation of the dry aerosol mass from the total aerosol mass – 30% error (Kaufman et al. 1986).
- Conversion to trace gases from the dry aerosol mass – 40% error (see Figs. 3 and 5).
- Integration on a whole area and emission time – 60% error (Ferrare et al. 1990).

These errors are errors in multiplicative factors (e.g., the relation between wet aerosol mass and optical thickness or trace gases and dry aerosol mass), as a result the final product "P" can be described as: $P = \Pi P_i$, where P_i are the multiplicative factors. The multiplicative error in P (e) can be described by:

$$eP = \Pi e_i P_i, \text{ and therefore } \quad e = \Pi e_i.$$

The accumulated r.m.s. error, is found from the logarithm of e ($\log e = \Sigma \log e_i$) and the r.m.s. error is:

$$\text{r.m.s.}(\log e) = \sqrt{[\Sigma(\log e_i)^2]} = 0.76. \rightarrow e \approx 2.$$

Therefore the estimate of the emission rate is within a factor of 2.

16.5.1.5 Application of the Techniques

Satellite measurements of the aerosol emission and the presence of fires was used to detect the rate of emission of particulates and trace gases from biomass burning. In the following an example is given of analysis of emission from biomass burning due to deforestation during the dry season in Brazil (a limited area 6.5–15.5° south and 55–67° west is analyzed currently). The analysis included the following steps:

Calibration of the AVHRR Visible and Near-IR Channels. These channels were calibrated using the calibration derived for 1987 by Kaufman and Holben (1990). The satellite data were first calibrated by the preflight calibration supplied by NOAA together with the data. The radiances in the visible and near-IR channels were further divided by 0.81, in order to compensate for the deterioration in the calibration of the two channels.

Smoke Analysis. The surface reflectance was determined from radiances recorded over areas where local smoke was not observed (i.e., uniform areas) and assuming that the aerosol optical thickness is zero. The meaning of this assumption is that the background smoke is considered as part of the background radiance that includes the surface reflectance. Therefore, the determination of the amount of smoke emitted per fire is based on the freshly emitted smoke, and on the observed fires. This analysis is applied whenever the fresh

smoke is easily observed and related to the fires from which it was emitted. In the State of Rondonia the range of surface reflectance in channel 1 was found to be 0.05–0.13, and in channel 2: 0.22–0.34. Similar reflectances were determined in other areas (e.g., Bolivia, Para, and Matto Grosso). The fresh smoke increased the radiance (normalized to reflectance units: $L' = \pi L/F_o\mu_o$ where F_o is the extraterrestrial solar flux and μ_o is cosine of the solar zenith angle) in channel 1 from 0.06–0.12 to 0.15–0.25; and in channel 2 from 0.16–0.26 to 0.18–0.32. The increase in the radiance in channel 1, corresponds to an increase in the aerosol optical thickness of 0.5–3.0, and the increase in channel 2 implies single scattering albedo values approaching 1 (see Tables 2 and 3). Therefore it is concluded that smoldering rather than flaming is the major contributor to the emission products that we see in Brazil.

Table 2. Examples of the results for the smoke area (A), the number of fires (N), the aerosol single scattering albedo (ω_o), and the aerosol mass per fire (M_{af}) for the state of Rondonia, Brazil, as analyzed from the AVHRR imagery

Date	A smoke area (km^2)	N number of fires	ω_o single scat. albedo	M_{af} aerosol mass /fire (t)
7.31.87			0.99	60
8.10.87	54,000	1361	0.99	15
8.11.87	75,000	2302	0.99	22
8.12.87	70,000	3597	0.99	11
8.20.87	130,000	2010	1.00	23
8.21.87	153,000	2036	0.99	40
8.22.87	43,000	1570	0.98	21
8.23.87	54,000	720	0.96	78
8.27.87	197,000	1929	0.96	58
9.01.87	36,000	760	0.98	52
9.08.87	27,000	1830	0.97	26
9.09.87	150,000	4709	0.97	21
Average quantity			0.98 ± 0.01	35 ± 20

Table 3. Average emission rates from different fire regions (the emission represents the fire emissions before the satellite pass, per fire)

Fire region	Central location		ω_o	Aerosol	CH_4	CO	CO_2
	Latitude	Longitude	single scat. albedo	mass/ fire (t)	mass/ fire (t)	mass/ fire (t)	mass/ fire (t)
Rondonia	12°S	62°W	0.98	35 ± 20	20	600	3500
Bolivia	14°S	64°W	0.97	55 ± 20	33	930	5500
Mato Grosso	11°S	57°W	0.99	43 ± 15	26	730	4300
Average			0.98	45 ± 20	26	750	4500

The uncertainty in the estimation of the trace gases is 70% for CH_4 and CO and 80% for CO_2.

Analysis of Emission Rates per Fire. Due to the derived high value of the single scattering albedo (0.98) the emission rates per fire summarized in Table 3 are based on the relationship between the emission of particulates and trace gases for smoldering conditions [Eqs. (1), (3), (5), and (7)]. Remote sensing of the emitted aerosol and its conversion to the emitted trace gases (CO, CH_4, CO_2, etc.) shows (see Tables 2 and 3) that on average each fire in the tropics contributes 45 t of particulates, 25 t of CH_4, 750 t of CO, and 4500 t of CO_2. These emission rates per fire are for the total emission (before and after the satellite pass during 1 day), based on the ratio of the emission before the satellite pass and the total emission of 0.5 (see Sect. 16.5.1.2). If the fire continues more than 1 day, it will be counted again in the second day, but also its emitted smoke will be measured in each day separately. Therefore, in this analysis, in each day a fire can be considered as an independent fire.

Fire Count. Fires were counted based on the radiative temperatures in channel $3 - T_3$ and $4 - T_4$ of the AVHRR. A fire was identified if the radiative temperatures T_3 and T_4 fulfilled the following criteria:

$$T_3 \geq 316 \text{ K}, T_3 \geq T_4 + 10 \text{ K and } T_4 > 250 \text{ K}. \quad (7)$$

The first criterion requires that in order that a pixel is considered to contain a fire (or fires), it has to be very hot (close to the 320 K saturation level). The second criterion requires that the radiative temperature has to be much larger in channel 3 than in channel 4 if the pixel contains a fire rather than a warm surface (bare soil or dry grass in the tropics may be as hot). The third criterion requires that the pixel does not include strongly reflective clouds in the 3.7-μm channel, which may saturate the 3.7-μm channel.

Subject to these criteria, fires were counted during 49 out of 77 days (July 4 till Sept 18) in the dry season in Brazil, for which data were available. The fire count for the area between 6.5 and 15.5° south and 55 and 67° west is shown in Fig. 8 as a function of the Julian date. In order to display the sensitivity of the fire count to the apparent temperature of the fire in the 3.7-μm channel, three thresholds for the first criterion in Eq. (7) were used: 316 K, 318 K, and 320 K (shown in accumulative form in Fig. 8). The high correlation between these three temperature ranges shows that the criteria identify fires, that there is a good correlation between small (or less hot) fires and larger (or hotter) fires. Decreasing the threshold further resulted in contamination of the fire count from warm surface areas. A total of 115,000 fires were counted. The cloudiness was also estimated from the satellite imagery for the same period. Clouds may hide part of the fires from the sensor, but they also may indicate the presence of rain and thus less fires (see Fig. 9). Due to the small correlation between clouds and fire, it was assumed in this analysis that the presence of fires is independent of the presence of clouds, and that clouds with reflectance larger than 0.4 in the visible do hide fires. Accounting for the cloudiness in each day for which fires were counted increased the total number of fires to 132,000. In Fig. 10 the fires counted in each individual day are plotted together with the number that is corrected for the effect of clouds. Extrapolating these results to the whole fire

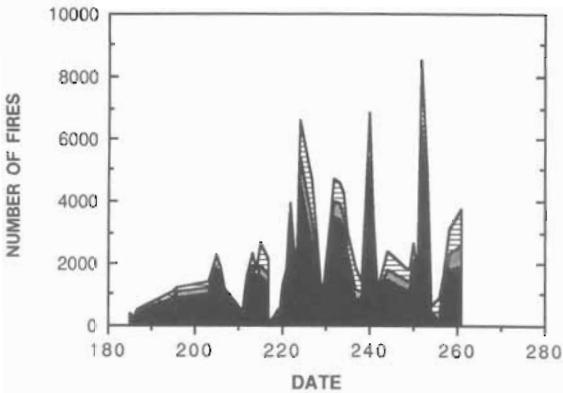

Fig. 8. Number of fires as a function of the day of the year for 1987. The fires were counted, based on the radiance in the AVHRR 1 km resolution imagery, in channels 3 and 4, over the area between 55 and 67° west, and 5.5 and 15.5° south. The *black area* represent fires that saturate channel 3 (3.7 μm), the *gray area* are additional fires that are 2 K colder, and the *dotted area* fires that are 4 K colder

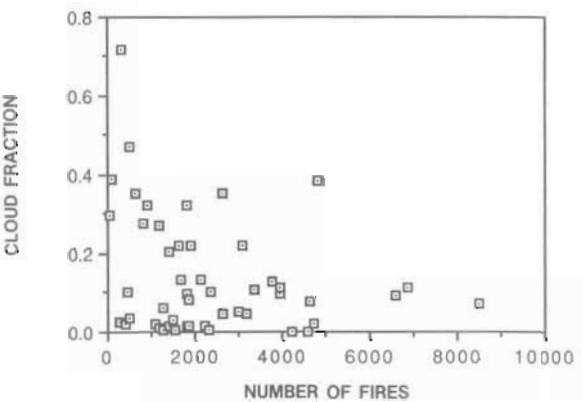

Fig. 9. Total cloud fraction as a function of the number of fires during the dry season in 1987, for the area between 55 and 67° west, and 5.5 and 15.5° south

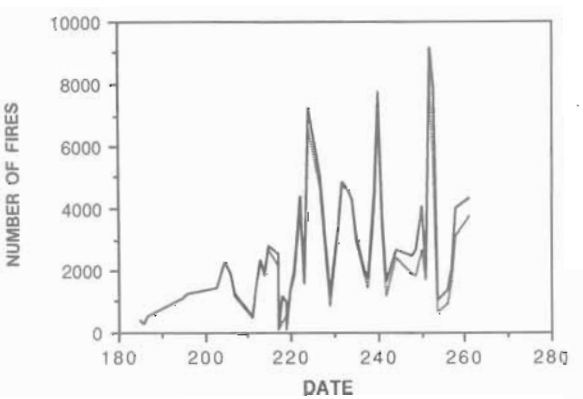

Fig. 10. Number of fires counted as a function of the day of the year for 1987 (*dotted line*) and corrected for the effect of clouds (*solid line*)

Table 4. Emission from biomass burning

Source	Particulates ($\times 10^{12}$g)	CH_4 ($\times 10^{12}$g)	CO ($\times 10^{12}$g)	CO_2 ($\times 10^{12}$g)
1. Estimate based on fire count and remote sensing of the aerosol (limited area: 6.5–15.5° south and 55–67° west)	11	7.3	180	1,100
2. Extrapolation of results in (1) to global deforestation in the tropics		73	1800	11,000
3. Estimate based on fire count and "average fire size" (area covering most of Brazil)		6	90	1,800
4. Global estimate (Crutzen et al. 1985)		40	800	10,000

Comparison to global budgets

Source	CH_4 ($\times 10^{12}$g)	CO ($\times 10^{12}$g)
Sources (Seinfeld 1986)	570–825	650–2200
Sinks (Seinfeld 1986)	605–665	1500–2500

season of 90 days, between July 1 and Sept. 31, we get 242,000 fires. Using the average emission rates per fire (in its present definition) from Table 3 we get total emission from the study area during the fire season shown in Table 4a.

16.5.2 Estimate Based on Average Biomass Burned per Fire

Forty six images from July 15 to October 2, 1987, were analyzed and pixels in band 3 corresponding to an AVHRR temperature reading above 315 K were selected as burning sites by a digital nonsupervised clustering algorithm. These pixels were next examined in the visible channel to verify if a smoke plume was associated with each of them; the image was also visually screened to ascertain if any significant plumes existed without a "fire pixel". Figure 7 corresponds to such an image for the area of the State of Randonia. The number of pixels thus classified was obtained for the Brazilian Amazon as well as for the individual states of the region. The most northern areas of the states of the Amazons and Para, and the Territory of Rorāima and the State of Amapa were not examined because they were out of the satellite range as viewed by the direct receiving station, which is located at about 23°S. Figure 11 shows thousands of fires burning along a belt from Belem, at the mouth of the Amazon River, to Porto Velho, capital of the State of Rondônia, stressing the current geographical limits of forest conversion in Brazil.

Table 5 presents a summary of the data obtained through 1987 and estimates of areas burned. The states of Acre and Maranhão had less frequent

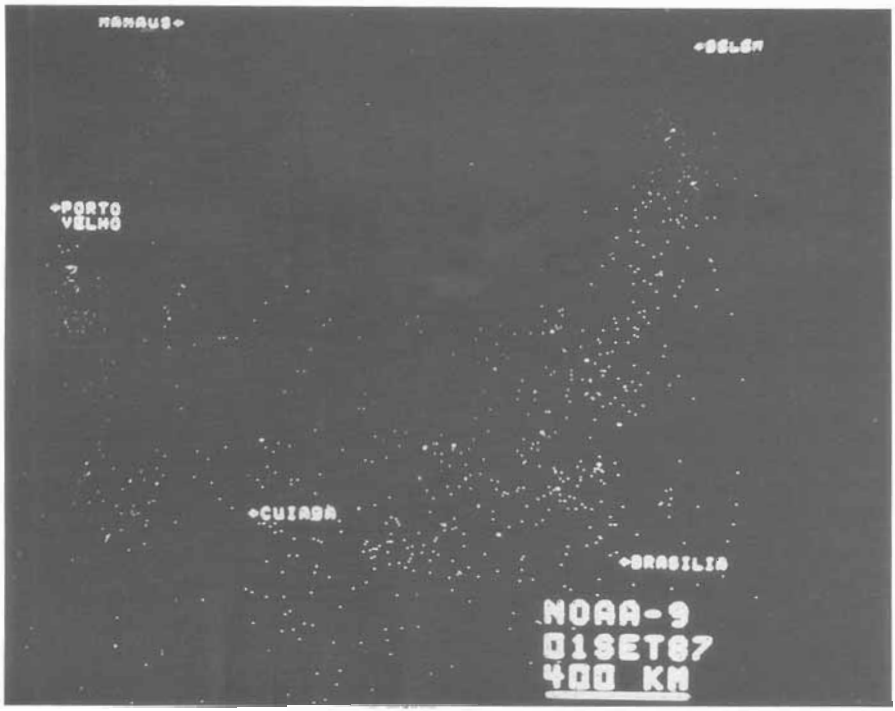

Fig. 11. Thousands of fires burning along a belt from Belem, at the mouth of the Amazon River, to Porto Velho, capital of the State of Rondônia, stressing the current geographical limits of forest conversion in Brazil

Table 5. Data summary of the 1987 burning/dry season

State	Acre	Mazonas	Para	Rondonia	M. Grosso	Goias	Maranhao	Total
Number of analyzed images	10	29	35	27	37	34	11	
Detected number of fire pixels	1557	679	14507	26267	62341	28338	3241	
Total number of fires	12456	1873	33159	77828	134791	66678	23571	350,000
Burned area (km^2)	7274	1094	19365	45452	78718	38940	13765	204,608

coverage because they appear at the far sides of the area of interest. "Average number of fire pixels" is the number of fire pixels registered in the images analyzed divided by the number of images; "total estimate of fire pixels" is the average number of fire pixels multiplied by 80, the number of days that the burning season is assumed to have lasted. In order to obtain the actual burned area some adjustments had to be made. First, some large fires lasted more than 1 day and were possibly registered twice by the satellite; field work information obtained in North Mato Grosso indicated 1.5 days to be a reasonable average value for areas in the 100-ha range, and the total number of fire pixels were adjusted by this factor. Second, in many cases the area actually burned, although smaller than a pixel, was depicted as a full pixel because of its high temperature. By comparing LANDSAT TM and NOAA-9 images for selected areas where burnings occurred also in North Mato Grosso, it was found that an overestimate of about 37% occurred in the NOAA-9 images, and therefore another adjustment factor was used. And finally, to obtain the corresponding burned areas, the adjusted pixel number was multiplied by 1.2, the area of a pixel in km^2 at nadir. These factors can certainly be elaborated to produce more precise figures, and the values issued represent a conservative estimate. As an example, the duration of fires is smaller for areas like the state of Rondônia where properties are usually in the 1–10-ha range. In this region the burned area overestimate is thus much larger, but many fires occur in the same pixel, and some small ones may be ended or not yet started when the image was obtained. Also, very dense smoke clouds from some fires may prevent the AVHRR from detecting other fires. As shown in Table 5, the total estimate of areas burned in the Brazilian Amazon basin in 1987 alone is about 200,000 km^2, close to five times the area occupied by the country of Switzerland. Of great importance is the knowledge of the percentage of this area that corresponds to recent forest conversion. This number also varies regionally, from 100% in regions of new development in the forest to a few percent for regions developed a few years ago or with predominant cerrado type vegetation (Setzer et al. 1988). As no statistics exist also in this case, the authors, based on limited field work activities and examination of LANDSAT TM images, suggest about 40%, or 80,000 km^2 as a conservative first guess. For the whole Amazon tropical forest this value must be greater, since other countries, such as Bolivia, are also pursuing deforestation policies.

Emissions of the 1987 burnings into the atmosphere were by no means small. Press reports relate that in the Amazon region and Central Brazil low visibility due to burnings that occurred hundreds of km away closed airports for many days, caused boat accidents in rivers, and also significant increases of respiratory diseases (Setzer et al. 1988). Carbon monoxide concentrations in remote areas of the Pantanal, thousands of km downwind from the main fires, increased by a factor of 10 (Kirchhoff et al. 1988). The smoke clouds were so large that they could be easily detected on the visible channel of images of the meteorological geostationary GOES satellite, and covered areas of millions of km^2 (Setzer et al. 1988).

An estimate of the fire emissions was made as follows. Based on Seiler and Crutzen (1980), the amount of dry matter burned can be estimated from

$M = A_i \times B_i \times ai \times b_i$, for i = 1 and 2, and where
M = Mass of dry matter burned, in g;
i = type of basic vegetation burned, where 1 is dense forest, and 2 cerrado;
A_i = Area of vegetation type i burned, in km^2
B_i = Average biomass of vegetation i, in g km^{-2};
a_i = Fraction of biomass over the soil in vegetation i; and,
b_i = Combustion factor for vegetation i.

If A1 = 40% and A2 = 60% of the estimated above, B_1 = 22.6 kg m^{-2} (Fearnside 1985), B_2 = 4.3 kg m^{-2} (Santos 1987), a_1 = 0.8 (Seiler and Crutzen 1980), a_2 = 0.65 (Santos 1987), b_1 = 0.6 (Setzer et al. 1988) and b_2 = 0.75 (Seiler and Crutzen 1980), resulting in $M = 1.15 \times 10^{15}$ g of dry matter burned in 1987.

Also following Seiler and Crutzen (1980), the associated emissions of carbon dioxide should be 45% of dry matter burned, or 0.52×10^{15} g, and based on the methodology presented by Andreae et al. (1988), the emissions of trace gases can be estimated, see Table 4a.

16.6 Discussion

The main advantage of the remote sensing method suggested in this chapter to sense the emission products from biomass burning in the tropics is in the availability of inexpensive and reliable daily satellite data (the NOAA-AVHRR) that provides information from every km^2 of the tropical forest on the number of fires and the smoke emitted by them. Since the 3.7-μm channel of the AVHRR is sensitive to fires as small as 10^{-4}–10^{-3} km^2 (10 × 10m of flaming or 30 × 30m of smoldering), it is possible to count all significant fires (unless there is more than one fire in a km^2 pixel), and detect new deforestation frontiers that could be gone undetected otherwise. The disadvantage of the relatively low saturation level of the AVHRR (320 K) that prevents one from distinguishing between small or large fires, and smoldering or flaming, is overcome by the ability of the satellite to detect the particulates emitted in the smoke from the fires, and to distinguish between smoke emitted from flaming fires and smoldering fires by the grayness of the smoke in the visible and near IR parts of the spectrum. Note that remote sensing of smoke by itself is not good to estimate the emission from biomass burning, due to the diffusiveness of the smoke and difficulties in smoke tracking (Ferrare et al. 1989). The main weaknesses in the present technique are in the integration on the emission time and in the transformation from particulates to trace gases. The time integration can be helped by analysis of GOES satellite imagery that can provide hourly information about the smoke (from its visible channel). The transformation from particulates to trace gases has to be studied by field measurement programs. Other uncertainties, such as the relationship between the measured radiance and the aerosol optical thickness, as well as the relationship of the optical thickness and the total and dry particulate matter can be reduced by in situ

measurements of the aerosol characteristics (e.g., size distribution) and meteorological conditions.

One unique characteristic of satellite-based techniques for monitoring biomass burning is the synoptic coverage of the data. The AVHRR polar orbiting sensors provide the basis for a global monitoring system. The techniques previously described in this chapter have been developed for the Amazon Basin where deforestation rates are high and forest burning is extensive. Other regions of tropical forest are undergoing various degrees of forest clearance through an increased demand for agricultural land. The techniques developed for the Amazon are currently being applied to other tropical regions of the World to test their general applicability for monitoring global biomass burning. Figure 12a is an AVHRR image of the northern boundary of the tropical forest of Equatorial Africa, including parts of Cameroun, Congo, Central African Republic, and Zaire. The major river systems are included in the image for geographic location. The image was derived from AVHRR channels 1, 3, and 4 to highlight the forest boundary and to reduce the effects of high cloud reflectance and warm land surfaces. The image shows a sharp contrast in brightness temperature between the tropical forest and the regrowth forest and

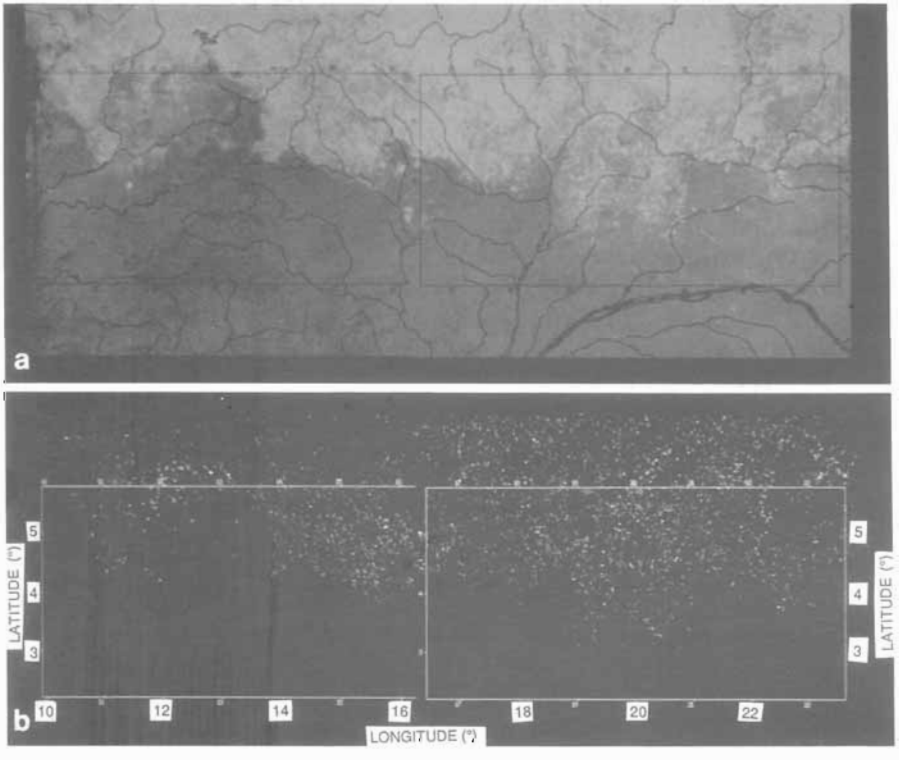

Fig. 12a,b. One week composite of the fire in Equatorial Africa, from the 3.7 μm channel of the 1 km

savannah mosaic. The image is a composite of five dates from January 1988 during the short dry season. Figure 12b is an enhanced image of the fire distribution for the same period. In this image 12,000 fires are depicted, the majority of which occur to the north of the forest margin within the mosaic of shifting agriculture and regrowth. The identification of fires within the savannah zone where there is extensive burning annually is a subject for further research and is complicated by the low saturation level of the AVHRR. Areas of active burning at the forest margin and within the forest domain can be identified and may provide evidence of active forest clearance. Preliminary analyses using these data are currently being undertaken to estimate the extent of biomass burning and to estimate the resulting gaseous emission within the entire equatorial forest region of Africa.

16.7 Conclusions

Deforestation and accompanying burnings in the Amazon are occurring at exponential rates which started in the early 1970's with the official policy to develop the region. Current yearly deforestation increases of 30% are expected for the states of Amazonas, Mato Grosso, Para, and Rondônia, where most deforestation takes place. If compared to a tentative evaluation of emissions for 1985 (Pereira 1988), the present estimate shows an increase of about 100% in the number of fires.

The burning emissions are in the lower troposphere, although some smoke clouds reach up to 4 km before starting to disperse horizontally. Considering that almost no rain occurs during the burning/dry season, the emissions enter the circulation of the anticyclonic cell that prevails in central Brazil during this period, and are transported to latitudes of 20 to 30°S over the Atlantic Ocean. In that region, increases in ozone tropospheric concentrations have been reported in a possible link with biomass burnings (Fishman and Larsen 1987). Also in this region, as seen in meteorological satellite images, tropospheric air can be lifted to high levels by convection associated with the subtropical jet stream, and which will eventually carry the emissions to Antarctic latitudes as corroborated by wind data. Biomass burning emissions from the Amazon basin present a substantial source of carbon dioxide and many atmospheric reactive gaseous compounds, and aerosols that provide catalytic surfaces for photochemical reactions, which could cause changes in the planet's climate and atmospheric chemistry.

Comparison with the global estimates of biomass burning (Crutzen et al. 1985; Table 4), shows that the Amazon region presently analyzed emits 1/10 of the global estimate of biomass burning (Crutzen et al. 1985). Extrapolation of the present results to global emission from deforestation can be performed by assuming that the ratio between the regional emissions reported by Houghton et al. (1987) for 1980, are also valid for 1987. According to Houghton et al. (1987) the presently studied area emitted carbon in the rate of 160×10^{12} g year^{-1},

while the global emission from tropical deforestation was 1650×10^{12} g year^{-1}. If the same ratios were applied for 1987, then the emission from tropical deforestation in 1987 are similar to estimates of total global emission from all types of biomass burning (deforestation as well as others) in 1980. This is mainly due to the expansion of deforestation and biomass burning due to population expansion, as found in the Amazon.

Acknowledgements. We would like to thank: Robert Chatfield from NCAR, Robert Fraser from NASA/GSFC, Jennifer Robinson from Penn State Univeristy, A.C. Pereira, F. Siquerira, G. Rodriqeus, J.C. Moreira, M.M. Cordeiro, P.C.D. Santos, and V.A.S. Oliveira, at INPE/Brazil, C. Paive and S. Almeida at IBDF/Brazil, J.P. Malingreau at EEC/Italy, and B.N. Holben at GIMMS/NASA. Darold Ward from the USDA Forest Service, for fruitful discussions throughout this study, as well as Jackline Kendall, Shana Matto, and Robert Rank for the software development and the image processing involved in this work.

References

Ackerman TP, Toon OB (1981) Absorption of visible radiation in atmosphere containing mixtures of absorbing and nonabsorbing particles. Appl Optics 20:3661–3668

Anderson IC, Levine JS, Poth M, Riggan PJ (1988) Enhanced emission of biogenic nitric oxide and nitrous oxide from semi-arid soils following surface biomass burning. J Geophys Res 93:3893–3898

Andreae MO, Browell EV, Garstang M, Gregory GL, Harris RC, Hill GF, Jaqcob DJ, Pereira MC, Sachse GW, Setzer AW, Silva Dias PL, Tablot RW, Torres AL, Wofsy SC (1988) Biomass burning emissions and associated haze layers over Amazonia. J Geophys Res 93:1509–1527

Atjay GL, Ketner P, Duvigneaud P (1979) In: Bolin B, Degens ET, Kempe S, Ketner P (eds) The global carbon cycle. Wiley, New York, pp 129–182

Blake DR, Rowland FS (1986) World-wide increase in tropospheric methane, 1978–1983. J Atmos Chem 4:43–62

Chatfield RB, Delany AC (1988) Efficiency of tropospheric ozone production: a tropical example of NO_x dilution and cloud transport. Presented at American Geophysical Union Fall Meeting, San Francisco, December 5–9, 1988

Coakley JA Jr, Cess RD, Yurevich FB (1983) The effect of tropospheric aerosol on the earth's radiation budget: a parametrization for climate models. J Atmos Sci 40:116

Coakley JA Jr, Borstein RL, Durkee PA (1987) Effect of ship stack effluents on cloud reflectance. Science 237:953–1084

Cofer WR, Levine JS, Riggan PH, Sebacher DI, Winstead EL, Shaw EF, Brass JA, Ambrosia VG (1988) Trace gas emissions from a mid-latitude prescribed chaparral fire. J Geophys Res 93:1653–1658

Crutzen PJ (1988) Tropospheric ozone: an overview. In: Isaksen ISA (ed) Tropospheric ozone. Reidel, Dordrecht, pp 3–32

Crutzen PJ, Graedel TE (1988) The role of atmospheric chemistry in environment-development interactions, Chapter 8. In: Clark WC, Munn RE (eds) Sustainable development of the biosphere. Cambridge Univ Press, Cambridge

Crutzen PJ, Heidt LE, Krasnec JP, Pollock WH, Seiler W (1979) Biomass burning as a source of atmospheric gases. Nature (Lond) 282:253–256

Crutzen PJ, Delany AC, Greenberg J, Haagenson P, Heidt L, Lueb R, Pollock W, Seiler W, Wartburg A, Zimerman P (1985) Tropospheric chemical composition measurements in Brazil during the dry season. J Atmos Chem 2:233–256

Dozier J (1980) Satellite identification of surface radiant temperature fields of subpixel resolution. NOAA Tech Mem NESS113, Washington DC

Fearnside PM (1985) Summary of progress in quantifying the potential contribution of Amazonian deforestation to the global carbon problem. In: Workshop on biogeographic of tropical rain forest, Piracicaba, SP, Brazil, Sep/30-Oct/04. Proceedings, CENA/USP, 1985, pp 75–82

Ferrare RA, Fraser RS, Kaufman YJ (1990) Satellite remote sensing of large scale air pollution – application to a forest fire. J Geophys Res (in press)

Fishman J, Larsen JC (1987) The distribution of total ozone and stratospheric ozone in the tropics: Implications for the distribution of tropospheric ozone. J Geophys Res 92:6627–6634

Fishman J, Minnis OP, Reichle HG Jr (1986) Use of satellite data to study ozone in the tropics. J Geophys Res 91:14451–14465

Fraser RS, Kaufman YJ (1985) The relative importance of scattering and absorption in remote sensing. IEEE Trans Geos Rem Sens 23:625–633

Fraser RS, Kaufman YJ, Mahoney RL (1984) Satellite measurements of aerosol mass and transport. J Atmos Environ 18:2577–2584

Greenberg JP, Zimmerman PR, Heidt L, Pollock W (1984) Hydrocarbon and carbon monoxide emissions from biomass burning in Brazil. J Geophys Res 89:1350–1354

GTC Global Tropospheric Chemistry (1986) UCAR, PO Box 3000, Boulder CO 80307

Hänel G (1981) An attempt to interpret the humidity dependencies of aerosol extinction and scattering coefficients. Atmos Environ 15:403–406

Houghton RA, Woodwell GM (1989) Global climatic change. Sci Am 260:36–44

Houghton RA, Boone RD, Fruci JR, Hobbie JE, Melillo JM, Palm CA, Peterson BJ, Shaver GR, Woodwell GM (1987) The flux of carbon from terrestrial ecosystems to the atmosphere in 1980 due to changes in land use: geographic distribution of the global flux. Tellus 39b:122–139

Kaufman YJ (1987) Satellite sensing of aerosol absorption. J Geophys Res 92:4307–4317

Kaufman YJ, Fraser RS (1983) Light extinction by aerosols during summer air pollution. J Appl Meteor 22:1694–1706

Kaufman YJ, Holben BN (1990) Calibration of the AVHRR visible and near IR sensors using molecular scattering, ocean glint and desert reflection. J Appl Meteor (in press)

Kaufman YJ, Sendra C (1988a) Satellite remote sensing of aerosol loading over land. In: Hobbs PV, McCormick MP (eds) Aerosols and climate. Deepak, Hampton, VA

Kaufman YJ, Sendra C (1988b) Algorithm for atmospheric corrections. Int J Rem Sens 9:1357–1381

Kaufman YJ, Brakke TW, Eloranta E (1986) Field experiment to measure the radiative characteristics of a hazy atmosphere. J Atmos Sci 43:1136–1151

Kaufman YJ, Tucker CJ, Fung I (1989) Remote sensing of biomass burning in the tropics. Adv Space Res 9:265–268

Kaufman YJ, Fraser RS, Ferrare RA (1990) Satellite remote sensing of large scale air pollution-method. J Geophys Res (in press)

Kirchhoff V, Setzer AW, Marinho E, Pereira MC (1988) Effects of forest burnings in the increase of CO over remote areas of Brazil. Brazilian Soc Adv Sci Congr, Oct 88

Malingreau J, Tucker CJ (1988) Large scale deforestation in the Southeastern Amazon Basin of Brazil. Ambio 17:49–55

Matson M, Dozier J (1981) Identification of subresolution high temperatures sources using thermal IR sensors. Photogr Engineer Rem Sens 47(9):1311–1318

Matson M, Schneider SR, Aldridge B, Satchwell B (1984) Fire detection using NOAA-series satellite. NOAA Technical Report NESDIS-7. Washington DC, Jan/84, 34 pp

Matson M, Stephens G, Robinson J (1987) Fire detection using data from the NOAA-N satellites. Int J Rem Sens 8:961–970

Mekler Yu, Kaufman YJ, Fraser RS (1984) Reflectivity of the atmosphere-inhomogeneous surface system: Laboratory simulation. J Atmos Sci 41:2595–2604

Mooney HA, Vitousek PM, Matson PA (1987) Exchange of materials between terrestrial ecosystems and the atmosphere. Science 238:926–931

Oltmans SJ, Komhyr WD (1986) Surface ozone distributions and variations from 1973–1984 measurements at the NOAA Geophysical monitoring for climatic change baseline observatories. J Geophys Res 91:5229 5236

Patterson EM, McMahon CK (1984) Absorption characteristics of forest fire particulate matter. Atmos Environ 18:2541–2551

Patterson EM, McMahon CK, Ward DE (1986) Absorption properties of graphitic carbon emission factors of forest fire aerosols. Geophys Res Lett 13:129–132

Pereira MC (1988) Detecção, monitoramento e analise de alguns efeitos ambientais de queimadas na Amazônia atraves da utilizaçã de imagens dos satelites NOAA e Landsat, e dados de aeronave. MSc dissertation: The Brazilian Space Research Institute/Ministry of Science and Technology- INPE/MCT, Publication No INPE-4503-TDL/326, May/88, 268 pp (in portugese)

Puschel RF, Livingston JM, Russell PB, Colburn DA, Ackerman TP, Allen DA, Zak BD, Einfeld W (1988) Smoke optical depths: magnitude, variability and wavelength dependence. JGR 93:8388–8402

Radke LF (1989) Airborne observations of cloud microphysics modified by anthropogenic forcing, AMS Symp Atmospheric Chemistry and Global Climate, Jan 29–Feb 3, Anaheim, CA 310–315

Radke LF, Hegg DA, Lyons JH, Brock CA, Hobbs PV, Weiss R, Rassmussen RA (1988) Airborne measurements of smokes from biomass burning. In: Hobbs PV, McCormick MP (eds) Aerosols and climate. Deepak, Hampton, VA

Ramanathan V, Cicerone RJ, Singh HB, Kiehl JT (1985) Trace gas trends and their potential role in climate change. J Geophys Res 90:5547–5566

Santos JR (1987) Analise preliminar da relaçã entre as repostas espectrais de dands TM/Landsat e a fitomassa dos cerrados brasileiros. In: II Symp Latino-Americano de Sensoriamento Remoto, Bogota, Colombia, May 16 20 (in press)

Seiler W, Crutzen PJ (1980) Estimates of gross and net fluxes of carbon between the biosphere and the atmosphere from biomass burning. Climate Change 2:207–247

Setzer AW, Pereira MC (1989) Amazon biomass burning in 1987 and their tropospheric emissions. (submitted to Ambio)

Setzer AW, Pereira MC, Pereira Jr AC, Almeida SAO (1988) Relatorio de atividades do projecto UBDF-INPE SEQE – ano de 1987. The Brazilian Space Research Institute/Ministry of Science and Technology-INPE/MCT, Publication No INPE-4534-RPE/565, May/88, 101 pp (in portugese)

Seinfeld JH (1986) Atmospheric chemistry and physics of air pollution. Wiley, New York, 738 pp

Stauffer R, Fisher G, Neftel A, Oeschger H (1985) Increase in atmospheric methane recorded in Antarctic ice core. Science 229:1386 1388

Tangren CD (1982) Scattering coefficient and particulate matter concentration in forest fire smoke. J Air Pollut Control Assoc 32:729–732

Tucker CJ, Holben BN, Goff TE (1984) Intensive forest clearing in Rondonia, Brazil, as detected by satellite remote sensing. Rem Sens Environ 15:255

Turco RP (1985) The photochemistry of the stratosphere. In: Levine JS (ed) The photochemistry of the atmosphere: Earth, the planets, and comets. Academic Press, Orlando, Florida, pp 77–128

Twomey SA (1977) The influence of pollution on the short wave albedo of clouds. J Atmos Sci 34:1149–1152

Twomey SA, Piepgrass M, Wolfe TL (1984) An assessment of the impact of pollution on the global albedo. Tellus 36b:356 366

Ward DE (1986) Field scale measurements of emission form open fires. Technical paper presented at the Defense Nuclear Agency Global effects review, Defense Nuclear Agency, Washington DC 20305-1000

Ward DE, Hardy CC (1984) Advances in the characterization and control of emissions from prescribed fires. 77th annual meeting of the Air Pollut Cont Ass, San Francisco, CA

Ward DE, Nelson RM, Adams DF (1979) Forest fire smoke plume documentation. 72nd annual meeting of the Air Pollut Cont Ass Cincinati, Ohio

Wayne RP (1985) Chemistry of the atmospheres. Clarendin, Oxford, 361 pp